

Minimum Detectable Defect Thickness in SPECT Myocardial Perfusion Test: Phantom Study with ^{99m}Tc and ^{201}Tl

Abdelhamid A. Elkamhawy and Harish Chandna

Nuclear Medicine, Department of Radiology, Cuero Community Hospital, Cuero, Texas

Objective: The purpose of this study was to determine experimentally the minimum thickness (D_{\min}) of a defect inserted on the myocardial wall of a cardiac phantom at different locations that could be clearly detected in a SPECT perfusion study using ^{99m}Tc and ^{201}Tl .

Methods: Rectangular (or cylindrical) defects with the same thickness were inserted on the inner surface of a myocardial phantom at 5 different locations: anterior (ANT), septal (SEP), inferoposterior (IP), lateral (LAT), and apical (AP). For different defect thickness (from 1 to 7 mm, in increments of 1 mm) the myocardial SPECT perfusion study was performed with ^{99m}Tc and ^{201}Tl using the same protocol that we use for patients. Baseline studies (with no defect inserted) were also performed. The SPECT images of the myocardial phantom with defects were compared with baseline SPECT images to determine whether the defect could be clearly identified.

Results: The uniformity of the baseline SPECT images was analyzed very carefully where an IP artifact was detected. The D_{\min} was determined for ^{99m}Tc and ^{201}Tl at 3 radii of rotation: 21.0, 25.0, and 29.2 cm.

Conclusion: To be detected on SPECT images, a defect must be of a thickness $\geq D_{\min}$. A simple method for performing a quality control test for SPECT nuclear cardiology can be developed based on these findings.

Key Words: SPECT; baseline SPECT images; minimum detectable thickness; external quality control test; inferoposterior artifact

J Nucl Med Technol 2001; 29:183-188

The left ventricle (LV) myocardial wall thickness ranges from 8 to 15 mm. To our knowledge, there has not been a conclusive study to assess the minimum perfusion defect thickness that can be detected by a SPECT test with ^{99m}Tc and ^{201}Tl . For follow-up patients, it becomes important to detect and assess a myocardial perfusion defect not involv-

ing the full LV wall thickness. In this cardiac phantom study, we determined the minimum detectable defect thickness at different locations within the myocardial wall.

MATERIALS AND METHODS

Cardiac Phantom

A cylindrical cardiac phantom (Data Spectrum Corp., Hillsborough, NC) with inner chamber diameter of 36 mm and length of 74 mm and outer chamber diameter of 60 mm and length of 86 mm was used to acquire the SPECT projection data. The space between the two chambers simulated the myocardial wall of the left ventricle (MWLV) and had a thickness of 12 mm and volume of 120 mL. The alignment pins, which were originally mounted on the outer wall of the inner chamber, were removed. Plastic defects were fixed on the outer wall of the inner chamber using a thin layer of Bulldog Grip glue (Drummond American Corp., Vernon Hills, IL), which worked perfectly in water solutions and was easy to remove. For SPECT studies the MWLV portion of the phantom was filled with 11.1 MBq (0.3 mCi) ^{99m}Tc water solution (1% of the patient dose) (1) or 4.44 MBq (0.12 mCi) of ^{201}Tl solution (4% of the patient dose) (2). To ensure uniform distribution, the tracer was mixed with water before filling.

Quality Assurance

The study was performed using a single-head gamma camera system (Genesys; ADAC, Milpitas, CA) with a low-energy, high-resolution (LEHR) parallel hole collimator. To increase the clinical usefulness of SPECT studies, we performed the following quality control tasks:

1. The camera was carefully peaked every working day at energy level of 140 keV (20% window) for ^{99m}Tc and at energy levels of 72 keV (25%), 135 keV (15%), and 167 keV (20%) before ^{201}Tl studies.
2. The intrinsic uniformity was measured daily using a point ^{99m}Tc source set at a distance of 310 cm from the center of the crystal, and the variation was always $<2\%$.
3. The intrinsic spatial resolution was checked weekly

For correspondence or reprints contact: Abdelhamid Elkamhawy, Nuclear Medicine Supervisor, Cuero Community Hospital, 2550 N. Esplanade, Cuero, TX 77954; Phone: 361-275-6191 (ext. 476); Fax: 361-275-9908; E-mail: abdel@dewittec.net.

using a 4-quadrant bar phantom and was always better than 3.2 mm.

4. The extrinsic spatial resolution of the system was evaluated by scanning a point ^{99m}Tc source (3) and using the count profile software program provided by the manufacturer. The point spread function (PSF) of the source (count density vs. pixel number) was obtained by generating a straight line through the source image. The extrinsic spatial resolution was determined by calculating the full width at half maximum (FWHM). The extrinsic spatial resolution was found to be 7.5 mm at the collimator surface and 8.7, 9.9, 11.6, and 13.9 mm at distances of 10, 21.0, 25.0, and 29.2 cm from the collimator, respectively.
5. The pixel size for the 64×64 matrix size and 38×38 cm² field of view, which is routinely used to acquire the cardiac SPECT studies, was measured weekly to be 5.8 ± 0.2 mm.
6. The axis of rotation was checked weekly using the software program provided by the manufacturer. The error range for both the *x*-axis and the *y*-axis was always less than 2 mm for the 64×64 matrix size and full field of view.

Acquiring and Processing

The phantom was scanned using the same protocol that is used for imaging a myocardial SPECT patient. Phantom was placed on the imaging table approximately at the center of gantry rotation so that the long axis made an upward angle of 10–15° with the table surface. No attenuating media was placed around the phantom. The projection data were acquired in 64×64 matrix for a circular 180° orbit from the left posterior oblique (135°) position to right anterior oblique (–45°) position in a step-and-shoot mode. Sixty-four images (20 s per image) were acquired for ^{99m}Tc , and 32 images (40 s per image) for ^{201}Tl studies. The raw data was processed by the AutoSPECT+ software program (ADAC, Milpitas, CA) using a gaussian filter (order, 5; cutoff frequency, 0.5 cycle/pixel). No attenuation or scatter correction was performed.

Baseline SPECT Images

The baseline SPECT phantom images were acquired for each radius of rotation (ROR) without any defects (inserts). These data were then used to compare the baseline images to the images with the defects inserted in the phantom. The baseline SPECT phantom images were also acquired using a 360° acquisition (64 images, 20 s per image) for circular (25.0-cm ROR) as well as elliptical (25.0-cm long-axis and 15.0-cm short-axis) orbits.

To estimate the degree of nonuniformity in baseline SPECT images, a bull's-eye map was generated and the region ratio software program provided by the manufacturer was used to determine the average ratio of count density for the anterior-to-inferoposterior (ANT/IP) regions as well as for the septal-to-lateral (SEP/LAT) regions.

Determination of Minimum Detectable Defect Thickness

For experimental determination of minimum detectable defect thickness in phantom SPECT studies, we performed the following steps:

1. We inserted 4 plastic defects (cylindrical or rectangular) of 50-mm length, 20-mm width, and a thickness (depth) of 7 mm, so that the long-axis of the strip was parallel to the phantom long-axis. These strips were fixed at four regions—anterior (ANT), septal (SEP), inferoposterior (IP), and lateral (LAT)—on the inner wall of the MWLV portion of the phantom. A fifth defect of $20 \times 20 \times 7$ mm³ was inserted to the apical (AP) region of the phantom. Figure 1 shows the defect locations inside the phantom. Note that all defects had the same thickness (or depth) for a given set of measurements.
2. The MWLV portion of the phantom was then filled with ^{99m}Tc water solution, and at three ROR (21.0, 25.0, and 29.2 cm) the SPECT studies were performed.
3. The phantom was refilled with ^{201}Tl water solution and step 2 was repeated.
4. The thickness of the 5 defects was decreased by increments of 1 mm, and steps 2 and 3 were repeated for every thickness.

RESULTS

Baseline SPECT Images

The tracer distribution within the baseline SPECT images was nonuniform, especially for ^{201}Tl . Figure 2 clearly shows this nonuniformity on short-axis, vertical long-axis, and horizontal long-axis baseline images with ^{201}Tl for 21.0-cm ROR, where a clear loss of count density is seen in the IP region near the base, which is an artifact. Table 1 shows the average density ratios ANT/IP and SEP/LAT for ^{99m}Tc and ^{201}Tl at three different ROR.

It was also found that the nonuniformity of the baseline SPECT images was independent of the arc of the acquisition orbit (180° or 360°), the orbit type (circular or elliptical), and the direction of rotation (clockwise or anticlockwise).

To verify that the IP defect was not specific to our camera, the same phantom was scanned without any inserted defects for ^{201}Tl for ROR = 21.0 cm using 2 other gamma camera systems: single-head ADAC Genysys (DeTar Hospital, Victoria, TX) and dual-head Sopa DSTXL (Citizens Medical Center, Victoria, TX), and in both cases the IP artifact with ^{201}Tl was detected.

Minimum Detectable Defect Thickness

Figure 3 shows the phantom SPECT images with ^{99m}Tc (row A) and ^{201}Tl (row B) at 29.2-cm ROR, where 5 defects with a thickness of $D = 6$ mm were inserted at the 5 locations described in Figure 1. This figure shows that the SPECT images with ^{99m}Tc were sharper than those with ^{201}Tl and that all defects were clearly seen with both tracers, except the defect located in the septal region, where it is

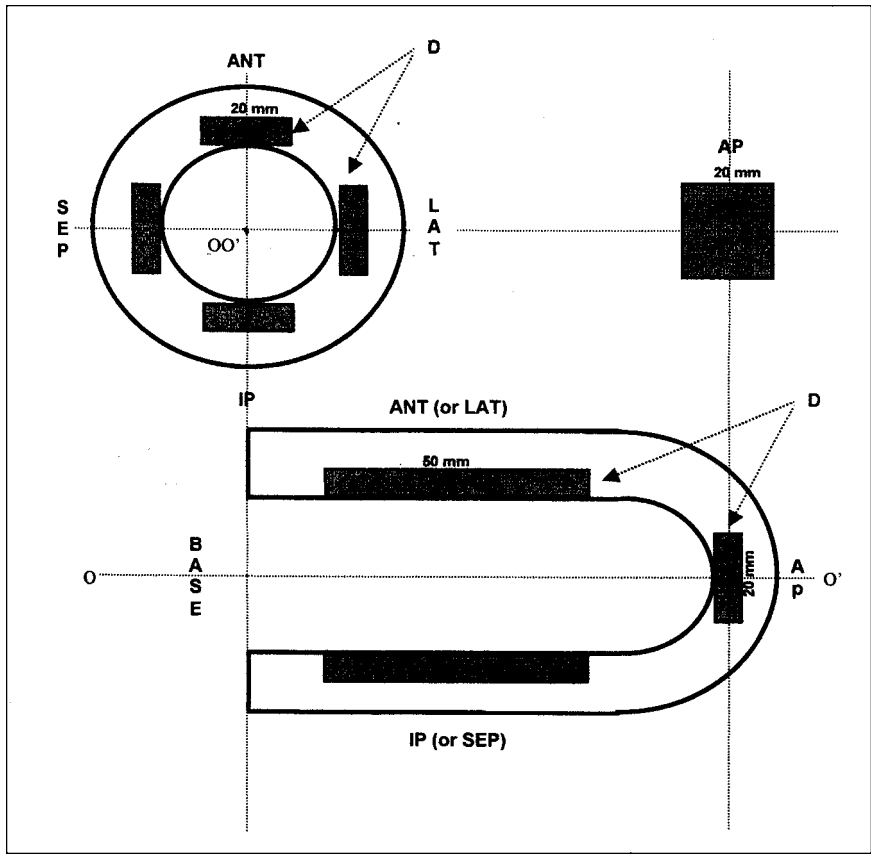


FIGURE 1. Locations of defects inside myocardial phantom. D = thickness (depth) of the defect.

seen on short-axis slices and barely seen on horizontal long-axis slices.

Table 2 summarizes the minimum detectable defect thickness (D_{min}) in SPECT images for ^{99m}Tc and ^{201}Tl as determined at 3 different ROR. D_{min} is expressed in millimeters and as a percentage of the phantom myocardial wall thickness. D_{min} is the minimum thickness of the defect at

which the defect can still clearly be seen on 2 different projections of SPECT slices, and below which the defect cannot be clearly detected. From Table 2 we notice:

- For the same location and same ROR, D_{min} is less with ^{99m}Tc than with ^{201}Tl .
- D_{min} is smallest when the defect is located in the IP region and greatest when the defect is located in the SEP region.

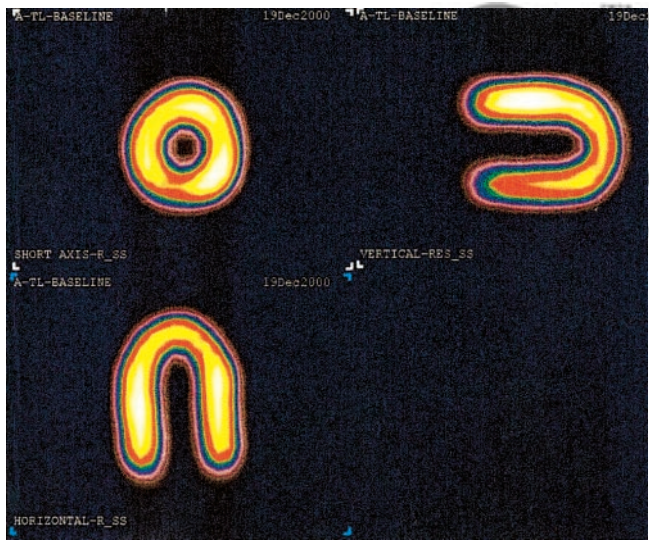


FIGURE 2. Example of short-axis, vertical long-axis, and horizontal long-axis slices showing nonuniformity of baseline SPECT images.

The phantom was scanned again to confirm the later result. The two 6-mL ($40 \times 50 \times 3 \text{ mm}^3$) defects were placed in the phantom in two opposing locations (ANT and IP), and rotating the phantom by 90° , the locations were changed to SEP and LAT. The SPECT images with both tracers at 25.0-cm ROR showed that the defects located in the IP region were the only ones that were clearly seen.

TABLE 1
Average Density Ratios for Baseline SPECT Images

| Isotope | ROR (cm) | Average density ratio | |
|------------|----------|-----------------------|---------|
| | | ANT/IP | SEP/LAT |
| ^{99m}Tc | 21.0 | 1.10 | 1.05 |
| | 25.0 | 1.07 | 1.05 |
| | 29.2 | 1.05 | 1.03 |
| ^{201}Tl | 21.0 | 1.18 | 1.05 |
| | 25.0 | 1.12 | 1.03 |
| | 29.2 | 1.08 | 1.01 |

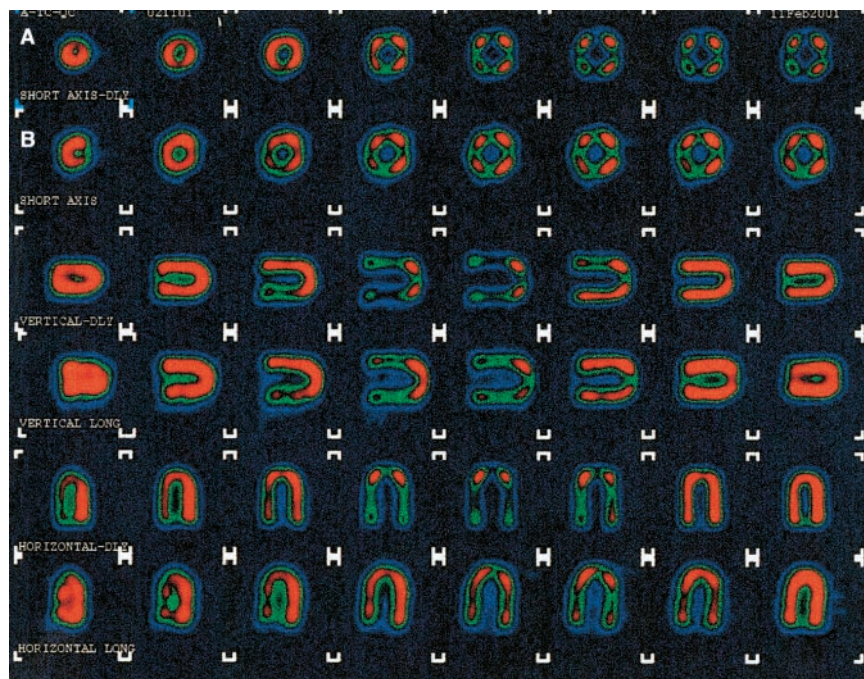


FIGURE 3. Phantom SPECT images for ROR = 29.2 cm, with ^{99m}Tc (row A) and ^{201}Tl (row B) where 5 defects with thickness $D = 6$ mm were inserted. All defects are clearly detected with both tracers except defect located in SEP region in ^{201}Tl study.

Figure 4 shows the phantom SPECT images with ^{99m}Tc and ^{201}Tl at 25.0-cm ROR, where approximately 2-mL defects ($22.5 \times 22.5 \times 4 \text{ mm}^3$) were located in the ANT, SEP, IP, and LAT regions midway between the apex and the base. All 4 defects were detected with ^{99m}Tc , whereas only the defect located in the IP regions was clearly seen with ^{201}Tl .

Figure 5 shows the phantom SPECT images with ^{99m}Tc at 25.0 cm ROR, where 2 defects of approximately the same volume (1 mL) but of different thicknesses (6 vs. 3 mm) were located at the ANT, SEP, IP, and LAT regions (2 defects for each region). The first defects of $13 \times 13 \times 6 \text{ mm}^3$ were located toward the apex, and the second defects of $18.5 \times 18.5 \times 3 \text{ mm}^3$ were located toward the base. The separation between the 2 defects was 10 mm. Row B on Figure 5 shows the phantom baseline SPECT images with ^{99m}Tc for 25.0-cm ROR. In Figure 5, the 6-mm-thick defects are clearly seen for all 4 regions, whereas the 3-mm-thick defects near the base are clearly visible only for the IP region.

DISCUSSION

The loss of counts in the inferior wall of SPECT images where no defect exists has been reported in phantom (4,5) and clinical (6) studies. Lowe et al. (4), in a thoracic phantom study that detected this artifact with ^{201}Tl , noticed that the defect margins in the inferior wall were less distinct in ^{201}Tl SPECT images when attenuating media were present. Ye et al. (5) performed an anthropomorphic phantom study with ^{99m}Tc and ^{201}Tl that used an attenuation correction and resolution recovery software program to correct for this artifact. They found that the uniformity of SPECT images in regions where no defect presented was improved in ^{99m}Tc studies, while remaining unchanged in ^{201}Tl studies.

Our results showed that the uniformity of phantom baseline SPECT images improved as ROR increased (Table 1) and that the appearance of the IP artifact was independent of orbit type, orbit arc, direction of rotation, and gamma camera type. These facts may indicate that this artifact is related to physical factors associated with imaging the phantom, such as:

TABLE 2
Minimum Detectable Defect Thickness for ^{99m}Tc and ^{201}Tl

| Isotope | ROR (cm) | D_{\min} (mm; percentage of myocardial phantom wall thickness) | | | | |
|-------------------|----------|--|---------|---------|---------|---------|
| | | ANT | SEP | IP | LAT | AP |
| ^{99m}Tc | 21.0 | 4 (33%) | 4 (33%) | 2 (16%) | 4 (33%) | 3 (25%) |
| | 25.0 | 4 (33%) | 4 (33%) | 2 (16%) | 4 (33%) | 4 (33%) |
| | 29.2 | 4 (33%) | 5 (43%) | 3 (25%) | 4 (33%) | 4 (33%) |
| ^{201}Tl | 21.0 | 6 (50%) | 6 (50%) | 3 (25%) | 5 (43%) | 4 (33%) |
| | 25.0 | 6 (50%) | 6 (50%) | 3 (25%) | 6 (50%) | 4 (33%) |
| | 29.2 | 6 (50%) | 7 (58%) | 4 (33%) | 6 (50%) | 4 (33%) |

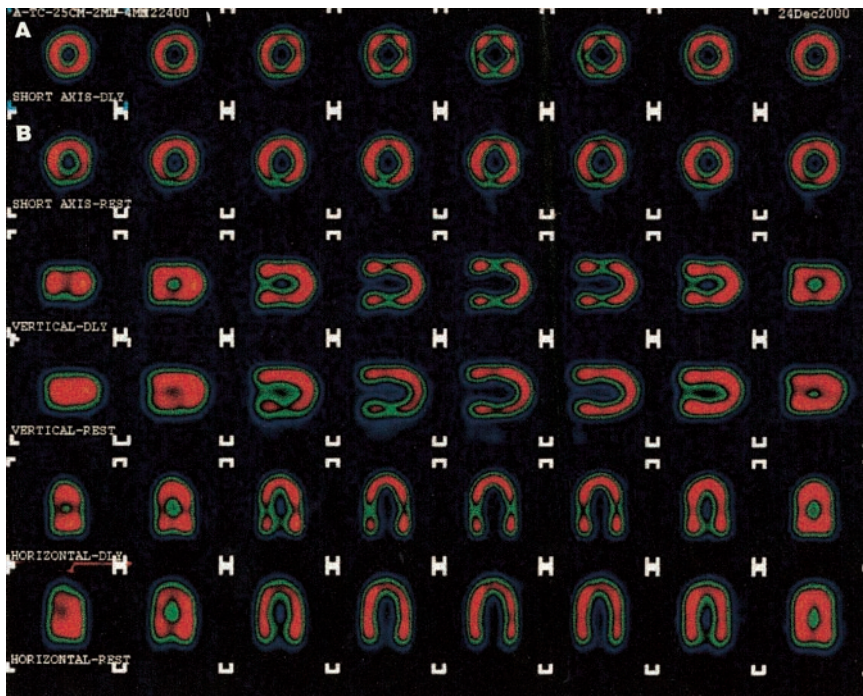


FIGURE 4. Phantom SPECT images with ^{99m}Tc (row A) and ^{201}Tl (row B) at ROR = 25.0 cm. Four defects of $22.5 \times 22.5 \times 4 \text{ mm}^3$ (~ 2 mL) were fixed at ANT, SEP, IP, and LAT regions. All defects were detected with ^{99m}Tc ; only the defect located in IP region was detected with ^{201}Tl .

1. Partial volume effect, since the phantom wall thickness is of a similar dimension to the spatial resolution of the gamma camera;
2. Degradation of spatial resolution as object-to-camera distance increases; or
3. Nonlinear attenuation of γ -rays through the phantom material.

All the preceding factors may produce regional reduction in the perfusion of baseline SPECT images, but do not explain the constant location of this artifact in the IP region.

Although cardiac diagnosis does not normally demand absolute quantification of defect size or severity, information about these quantities is important for the follow-up of cardiac patients.

The values of D_{\min} given in Table 2 cannot be extrapolated to real clinical studies because of the lack of cardiac and respiratory motion, absence of attenuation and scatter media, and the absence of gamma background from nearby organs in the phantom experiment.

Several software techniques have been developed to de-

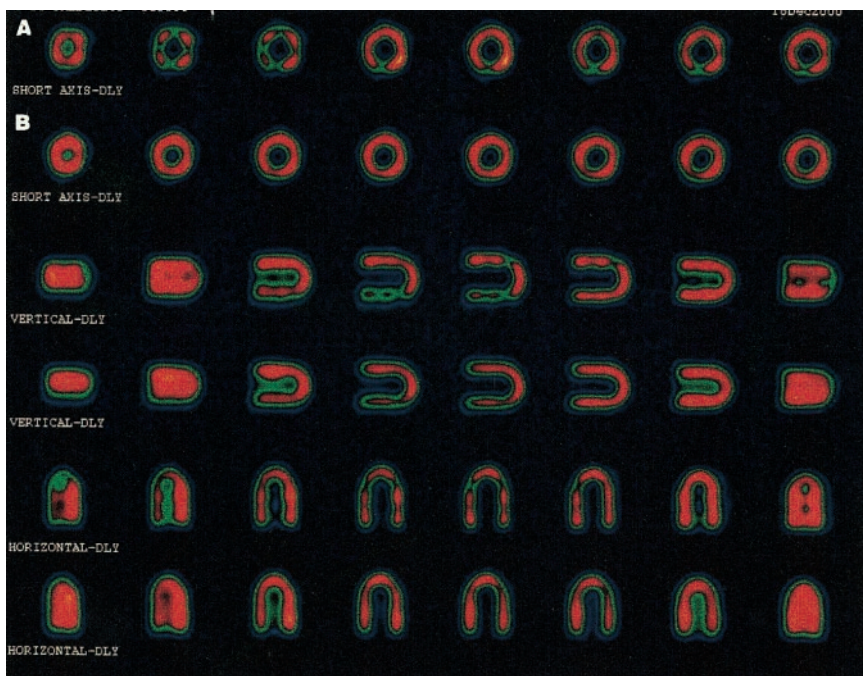


FIGURE 5. Phantom SPECT images for ROR = 25.0 cm with ^{99m}Tc (row A). Two 1-mL defects were inserted into ANT, SEP, IP, and LAT regions. All 6-mm defects are clearly seen; 3-mm defects are visible in IP region only.

termine defect size and severity (4,7,8) using cardiac SPECT perfusion images. O'Connor et al. (7) in their multicenter study with cardiac phantoms, analyzed 5 representative short-axis slices of ^{99m}Tc perfusion SPECT images to determine defect size and severity. They used 8 defects of relatively large volumes (5%–70% of the myocardial phantom volume) and reported that the error in defect size determination was <2%. Benoit et al. (8) used a 360° elliptical sampling of radial slices to evaluate defect size and severity in their Data Spectrum phantom study and in clinical studies. In the phantom study they used 7 defects with volumes of 6–48 mL to evaluate the software performance, and the defect size appeared to be accurately estimated, with mean relative standard deviation (RSD) of <8%. Lowe et al. (4), in their thoracic phantoms study to evaluate the dual-isotope (^{201}Tl rest/ ^{99m}Tc -sestamibi stress) technique, used the bull's-eye program to determine perfusion defect size and severity where 3 defects with volumes of 4.9, 9.5, and 19.2 mL were used. In this study the absolute error in determining the defect size for a single agent (^{99m}Tc or ^{201}Tl) increased as volume size decreased (for ^{99m}Tc without attenuation media, the absolute error was 8% for the 19.2-mL defect and 37% for the 4.9-mL defect). Our results showed that the appearance of small defects (1–4 mL) in SPECT images depends on defect thickness, defect location, acquisition ROR, and tracer type (^{99m}Tc or ^{201}Tl), especially when the defect thickness approaches D_{\min} . A correction factor may have to be introduced in software programs designed to determine defect size and severity.

Our experiment showed that D_{\min} is smallest (easiest to detect) for defects located in the IP region and greatest for defects located in the SEP region. This finding correlates well with the clinical results of Meyers et al. (9), in which the specific locations of cardiac wall abnormalities were assessed in a population of 562 patients with CAD using the dual-isotope perfusion (^{201}Tl rest/ ^{99m}Tc -sestamibi stress) test. The authors found that the largest percentage (35%) of defects were recorded for the inferior wall, whereas only 13.8% were found on the septal wall.

Heikkinen et al. (10) reported the results of a multicenter study to evaluate the quality of cardiac perfusion SPECT procedures in Finland that showed the need for an external quality control test in nuclear cardiology (in addition to the traditional SPECT QC test of uniformity, relative sensitivity, axis of rotation, pixel calibration, and spatial resolution). They also recommended the use of a LEHR collimator, 4–6 mm pixel size, the location of the myocardium closer to the center of rotation (COR), and the use of corrections for COR, uniformity, and attenuation.

Approximately 70%–75% of our workload in the nuclear medicine department is cardiac perfusion SPECT with ^{99m}Tc cardiolite and ^{201}Tl . For the external or overall QC test we suggest the configuration of defects shown on Figure 1, with a defect thickness of 6 mm. The phantom wall cavity is filled with 11.1 MBq of ^{99m}Tc water solution (or 4.44 MBq of ^{201}Tl solution) and the SPECT data are acquired at

25.0-cm ROR with 10 s per step for ^{99m}Tc and 20 s per step for ^{201}Tl . All defects were clearly seen on the reconstructed SPECT images using this procedure. This QC procedure takes 11 min to perform before acquisition of our clinical cardiac studies. Any deviation in the appearance of SPECT images may indicate a problem that should be corrected before acquiring patient data.

CONCLUSION

This study showed that defect thickness and location are important factors determining whether a defect would be detected in phantom myocardial perfusion studies. For a defect to be detected, it must have a threshold value $\geq D_{\min}$, which depends on the defect location within the myocardial wall, the acquisition ROR, and the tracer type (^{99m}Tc or ^{201}Tl). It was planned to use this phantom as a part of our QC procedure. The primary benefit obtained from this study was the determination of the best defect thickness for performing the QC procedure. This is a simple method for rapidly performing a QC test that is directly applicable to nuclear cardiology.

ACKNOWLEDGMENTS

The authors thank the administration of Cuero Community Hospital, Cuero, TX, for supporting the research in all its stages. We thank Professor Hussein M. Abdel-Dayem, MD; Steven C. Schnicker, MD; Stephen W. Tibbits, MD; James F. Neuman, MD; and Ajay K. Gaalla, MD, for fruitful discussions; and J. D. Davis and Judy Heil for help with manuscript preparation.

REFERENCES

1. Taillefer R, Tomaki N. *New Radiotracers in Cardiac Imaging: Principles and Applications*. Stamford, CT: Appleton & Lange; 1999:9.
2. Early PJ, Sodde DB. *Principles and Practice of Nuclear Medicine*. 2nd ed. St. Louis, MO: Mosby Year Book, Inc.; 1995:112.
3. Sorenson JA, Phelps ME. *Physics in Nuclear Medicine*. 2nd ed. Philadelphia, PA: Saunders; 1987:365–366.
4. Lowe VJ, Greer KL, Hanson MW, Jaszczak RJ, Coleman RE. Cardiac phantom evaluation of simultaneously acquired dual-isotope rest thallium-201/stress technetium-99m SPECT images. *J Nucl Med*. 1993;34:1998–2006.
5. Ye J, Liu L, Braymer W, Buskard T. Improvement in myocardial defect contrast and uniformity for SPECT in an anthropomorphic phantom using attenuation correction and resolution recovery for Tc-99m and Tl-201 [abstract]. *J Nucl Med*. 1998;39:180.
6. Normand B, Maublant J, D'Agrosa MC, Lusson JR, Veyre A. Comparison of the myocardial distributions of 201 Tl and 99m Tc MIBI on SPECT images. *Nucl Med Commun*. 1991;12:393–396.
7. O'Connor MK, Leong LK, Gibbons RJ. Assessment of infarct size and severity by quantitative myocardial SPECT: results from a multicenter study using a cardiac phantom. *J Nucl Med*. 2000;41:1383–1390.
8. Benoit T, Vivegnis D, Foulon J, Rigo P. Quantitative evaluation of myocardial single-photon emission tomographic imaging: application to the measurement of perfusion defect size and severity. *Eur J Nucl Med*. 1996;23:1603–1612.
9. Meyers A, Ballow J, Topham L, Rainer R, Field C. Assessing coronary artery disease with thallium-201 rest and technetium-99m-sestamibi stress testing at two centers. *J Nucl Med Technol*. 2000;28:248–251.
10. Heikkinen J, Ahonen A, Kuikka JT, Rautio P. Quality of myocardial perfusion single-photon emission tomography imaging: multicentre evaluation with a cardiac phantom. *Eur J Nucl Med*. 1999;26:1289–1297.